

# Increased surface flashover voltage in microfabricated devices

R. C. Sterling,<sup>1</sup> M. D. Hughes,<sup>1</sup> C. J. Mellor,<sup>2</sup> and W. K. Hensinger<sup>1</sup>

<sup>1</sup>*Department of Physics and Astronomy, University of Sussex, Brighton, BN1 9QH, UK*

<sup>2</sup>*School of Physics and Astronomy, University of Nottingham,  
University Park, Nottingham, NG7 2RD, UK*

Micro- and nano-fabricated devices have ground breaking impact in many areas of modern technology. With the demand for improved performance, the necessity to apply greater electric fields and voltages becomes evident. When operating in vacuum, the voltage is typically limited by surface flashover forming along the surface of a dielectric. By modifying the fabrication process we have discovered it is possible to more than double the flashover voltage. Our finding has significant impact on the realization of next-generation micro- and nano-fabricated devices and for the fabrication of on-chip ion trap arrays for the realization of scalable ion quantum technology.

Microfabricated devices such as NEMS and MEMS operating in vacuum have a multitude of applications. These include space application such as nanoelectrospray thruster arrays for spacecraft [1–4] and spacecraft solar arrays [5–7] to earth bound applications such as field emitter arrays. Most recently they have become a crucial tool for the realization of new quantum technologies based on ion traps. Ion traps have proven themselves to be a powerful tool for many experiments in modern science. They exhibit good isolation from the surrounding environment and long coherence times are achievable [8]. As a result ion trap experiments have been used to explore cavity QED [9, 10], the measurement of frequency standards [11], quantum simulators [12, 13] and quantum information processing [8, 14, 15]. The Paul ion trap has been used to demonstrate unparalleled success towards the implementation of the first scalable quantum computer, meeting most of the requirements for qubit control and extensive work is being carried out towards a scalable architecture within which to store and control the qubits [16].

However there still remain many challenging technical issues to address before a fully scalable ion trap quantum computer can be built. Not least is building an architecture within which thousands of ions may be stored, shuttled and manipulated. Recent work has focused on using microfabrication techniques to build ion trap arrays, harnessing the massive parallelism and accuracy achievable with modern semiconductor fabrication facilities [16]. This has lead to many advancements such as state manipulation from integrated microwave waveguides [17] and integrated optical fibers [18]. Despite these exciting advances there still remain several fundamental problems with microfabricated traps. A small ion-electrode separation is inherent to any micro-fabricated surface electrode trap geometry due to the limited voltages that can typically be applied. This leaves the ion susceptible to any uncontrolled charges collected on exposed dielectrics. These effects will have a slow time dependance and make

effective long term compensation troublesome. In order to minimize exposed regions of dielectric, electrodes are fabricated with only small gaps, on the order of several micrometers. Alternatively dielectrics can be successfully shielded completely from the ion using multi-layered geometries, but again microfabrication considerations limit layer thicknesses to a few micrometers. This results in large electric fields between electrodes and if proper care is not taken electrical breakdown can occur, destroying the chip.

Additionally the close proximity of the ion to the electrode surface induces anomalous heating of the ion's motional state, which scales approximately as  $d^{-4}$ , where  $d$  is the ion-electrode separation [19]. There have been several techniques demonstrated recently which manage to suppress the heating rate by performing surface cleaning [20, 21] or operating at cryogenic temperatures [22], but additional improvements can be made by designing traps with an increased ion-electrode separation. This also has benefits in easing optical alignment across the trap surface, reducing unwanted laser scatter from trap electrodes and reducing the effect of uncontrolled charging of dielectrics and electrodes [23].

For these reasons high fidelity operations are more difficult with microfabricated ion traps as they currently lack the benefits afforded to macroscopic traps. It is therefore desirable to find ways in which microfabricated ion trap arrays can be optimized in order to not only to improve their functionality, as seen in Refs. [16–18, 24], but also allow for larger voltages that can be applied so that larger ion-electrode distances can be used and smaller electrode-electrode spacings are possible. In this letter we present a simple method to significantly increase the voltage that can be applied to MEMS and microfabricated devices in general and on-chip ion trap arrays in particular. By increasing the maximum voltage before surface flashover occurs, traps can be designed with increased ion-electrode separations and smaller spacings between adjacent electrodes. We first investigate the differ-

ence between static and rf breakdown and then show how to modify the fabrication process to significantly increase the breakdown threshold.

Electrical breakdown in vacuum, also known as surface flashover, is described by secondary electron emission avalanche (SEEA) across the dielectric surface. Electrons hop across the dielectric surface which desorbs gas molecules from the surface leading to a Townsend-like breakdown through this gas layer [25–27]. This is a function of the amount of desorbed gas per  $\text{m}^2$  at the point of flashover,  $M_{cr}$ , the electron emission and impact energies,  $A_0$  and  $A_1$  respectively, the efficiency of electron stimulated gas desorption,  $\gamma$ , molecule ejection velocity,  $v_0$ , electron velocity,  $v_e$ , which is given by  $v_e = 5.94 \times 10^5 \sqrt{A_1} \text{ ms}^{-1}$  [26] and  $\theta$  which is the angle that electrons are emitted from the triple point, which is the point at which the dielectric, cathode and vacuum meet and is given by  $\tan \theta = [2A_0/(A_1 - A_0)]^{\frac{1}{2}}$  [26]. The flashover voltage is given by [26]

$$V_b = \left[ \frac{\varphi d e}{2\epsilon_0} \right]^{\frac{1}{2}} \quad (1)$$

where

$$\varphi = \frac{v_0 M_{cr} A_1}{\gamma v_e \tan \theta},$$

where  $d$  is the electrode separation,  $e$  is the electron charge and  $\epsilon_0$  is the permittivity of free space.

Unfortunately there is only a limited amount of information regarding  $M_{cr}$ ,  $\gamma$  and  $v_0$ , with measurements ranging over several orders of magnitude for different experimental setups [25–28], and  $A_1$  is only known for a handful of common dielectrics [29]. Therefore we will treat  $\varphi$  as a fitting parameter to compare between static and rf measurements and between different fabrication processes.

In order to set a base line for surface flashover, test samples were fabricated using a common, simple fabrication technique of gold electrodes deposited onto quartz. The electrodes were deposited by e-beam evaporation, depositing a chromium seed layer followed by a 500 nm layer of gold. Electrodes were patterned using standard photolithography and formed using wet etching. The electrodes were separated by gaps from 3 to 15  $\mu\text{m}$  in 2  $\mu\text{m}$  steps. The test chips were superglued to a ceramic chip carrier and connections made by wire bonding 30  $\mu\text{m}$  gold wire between the electrodes and chip carrier. The chip carrier was attached to a high power vacuum feedthrough and mounted inside a glass belljar. The system was evacuated using a turbomolecular pump to a pressure of  $1 - 8 \times 10^{-6}$  Torr. Static voltage was applied by attaching a 5 kV supply to

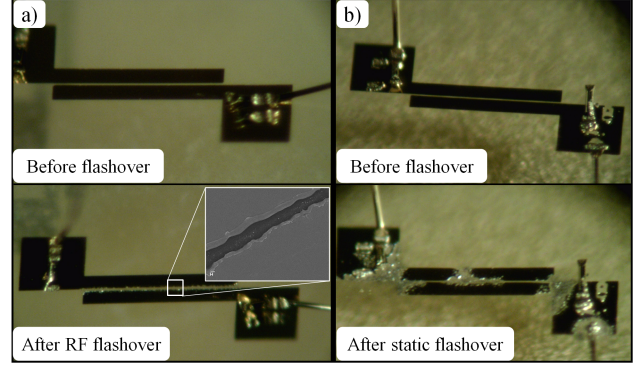


Figure 1: Samples before and after a flashover measurement is taken. (a) Picture showing a sample with 7  $\mu\text{m}$  electrode spacing before and after RF flashover occurred. The insert shows an electron microscope image of the damaged electrodes. (b) Picture showing a sample with 7  $\mu\text{m}$  electrode spacing before and after static flashover occurred.

the feedthrough with an in built voltage divider supplying a 0-10 V monitor voltage that could be measured by a calibrated voltmeter, with an error of  $\pm 10$  mV, resulting in an experimental error of  $\pm 5$  V. RF voltage was applied by attaching a 2  $\mu\text{H}$  inductor to the feedthrough forming a resonant LCR circuit with the chip, the resonant frequency of the inductor-chip circuit was  $22.0 \pm 0.5$  MHz. A 30 W amplifier was connected to the inductor via a bidirectional coupler with a capacitive probe measuring the voltage applied to the sample. Breakdown was measured by slowly ramping up the voltage while observing the sample through a lens, upon flashover a bright plasma discharge develops and the voltage ramp is stopped. The voltage is then recorded and the error of this measurement is  $\pm 7\%$  for both static and rf measurements.

Figure 1 shows four microscope images of test samples. Fig. 1(a) shows a 7  $\mu\text{m}$  gap before and after rf surface flashover, the inset shows a electron microscope image of the damaged electrodes. Figure 1(b) shows a 7  $\mu\text{m}$  sample before and after static flashover occurred. A significant visual difference can be observed. For rf flashover the closest edge along the full length of the electrodes has been eroded until flashover can no longer be sustained. This differs from static breakdown which occurs at the sharp edges of the electrodes where the E-field is strongest. Upon breakdown there is a sudden reduction in impedance and a rapid discharge of capacitively stored charge. This leads to large portions of the electrodes being destroyed during flashover. There are a number of mechanisms that may pre-

vent such damage for rf flashover. Plasma dissipation during the low voltage periods in the oscillation, when the electric field switches polarity may limit this damage. Another explanation relates to the Q-factor of the resonant rf circuit. When flashover occurs the resulting resistive component of the LC resonator circuit will rapidly lower the Q of the RF resonator and may stop the discharge. However once the discharge is stopped the Q increases again and so flashover re-occurs.

The results for both static and rf flashover are shown in Fig. 2 along with a plot of Equ. 1 using  $\varphi$  as a fitting parameter.

Equation 1 was solved for both the rf and static flashover data giving  $\varphi_{rf} = 4.62 \pm 0.10 \times 10^{18} \text{ eV m}^{-2}$  and  $\varphi_{dc} = 4.88 \pm 0.19 \times 10^{18} \text{ eV m}^{-2}$ . This represents a difference of  $\approx 5\%$  between rf and static flashover voltage showing no significant difference in breakdown voltage, despite the visual differences.

In order to increase the voltage when flashover occurs we have investigated other dielectric materials and discovered it is possible to substantially change the voltage at which flashover occurs. Silicon nitride is a common alternative to silicon dioxide and is readily available in microfabrication cleanrooms. Using plasma enhanced chemical vapor deposition (PECVD) alternating 80 nm thick layers of aSiO<sub>2</sub> and aSiN were deposited at 250°C in an isothermal PECVD reactor (Corial D250) onto a silicon substrate. The layered structure was formed to test bulk breakdown but for surface flashover only the top aSiN layer is of interest. The electrodes were formed by thermally evaporating a titanium adhesion layer followed by 200 nm of gold, then using lift-off to form the electrode geometry. The Au-nitride flashover measurements were performed at electrode separations of 5, 10 and 20  $\mu\text{m}$  with static voltage and are shown in Fig. 3, individual measurements are shown as empty diamonds with the mean as solid diamonds. It is clear that there is a significant increase in flashover voltage for all the measurements performed on aSiN with a  $\varphi = 29.2 \pm 2.6 \times 10^{18} \text{ eV m}^{-2}$ , meaning there is approximately a 2.5 times increase in flashover voltage for electrodes fabricated on aSiN compared to aSiO<sub>2</sub>. This fit was performed only for measurements taken at 5 and 20  $\mu\text{m}$  as there is an uncharacteristic dip in flashover voltage at 10  $\mu\text{m}$ , likely a result of a fabrication mask defect.

Since the electrodes for the aSiN samples were fabricated using a lift-off process we performed further measurements using the same fabrication process but on a quartz wafer in order to confirm that the increase in flashover voltage was a result of the dielectric material and not because of a change in the electrode deposition technique. Five measurements were taken between bond pad electrodes separated

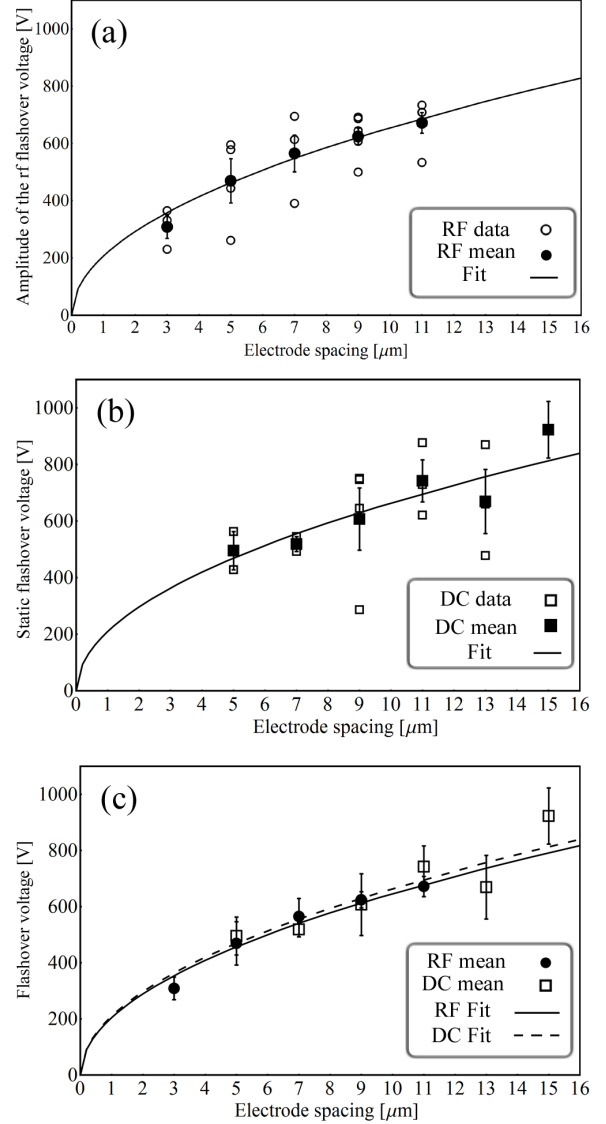


Figure 2: a) The amplitude of the rf flashover voltage data is shown as empty circles, the mean flashover voltage is shown as a solid circle.

Equation 1 is fitted to the data with  $\varphi_{rf} = 4.62 \pm 0.1 \times 10^{18} \text{ eV m}^{-2}$ . b) Static flashover voltage data is shown as empty squares, the mean flashover voltage is shown as solid squares.

Equation 1 is fitted to the data with  $\varphi_{dc} = 4.88 \pm 0.19 \times 10^{18} \text{ eV m}^{-2}$ . c) RF and static flashover electric field measurements. The rf mean is shown as circles with the static mean as empty squares. Equation 1 is plotted for both the rf and static voltage measurements, the fit for rf voltage measurements is shown as a solid line and the fit for static voltage measurements is shown as a dashed line.

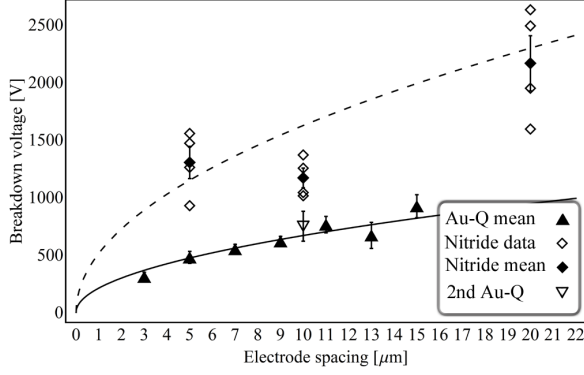


Figure 3: PECVD nitride flashover measurements are shown as empty diamonds, the average flashover voltage is shown as a solid diamond, with a fit using Equ. 1 shown as a dashed line, with  $\varphi$  as a fitting parameter. Flashover measurement for the Au-quartz samples are shown as solid triangles, these are an average of both the rf and static measurements, with a fit line shown as a solid line. The average of the second set of Au-quartz measurements is shown as an empty inverted triangle and shows good agreement with the first set of data.

by 10  $\mu\text{m}$  from an ion trap mask. The mean of these measurements is shown in Fig. 3 as an empty inverted triangle. It can be seen to agree with the first set of measurements, suggesting that there is no significant difference in flashover voltage as a result of using lift-off as opposed to wet etching.

We have demonstrated that by using silicon nitride instead of silicon dioxide as a dielectric in microfabricated devices the flashover voltage in vacuum can be significantly improved. This not only has applications for ion trap arrays but also for

other microfabricated and MEMS devices operating in vacuum such as nanoelectrospray thruster arrays for spacecraft [1–4] and spacecraft solar arrays [5–7], where high electric fields are desired. Further improvements may also be found by adjusting sample preparation prior to testing.  $\varphi$  is a function of not only dielectric material but also the density of adsorbed gas molecules. Processes to lower this density may further increase flashover voltage. These results offer new opportunities for the improvement of surface ion trap technology towards scalable architectures. Our results show that the separation between electrodes can be reduced, in principle, by a factor as large as 6 by incorporating the findings of our work in the fabrication process. This also greatly reduces potentially exposed dielectric surface area in ion trap arrays. Our results are also very promising for many other microfabrication applications such as MEMS, NEMS, quantum devices, field emitter arrays and space technology.

#### Acknowledgements

The authors would like to thank D. Brown and K. Schwab for fabricating the first gold on quartz test samples and James Sivers, Simon Webster and Sebastian Weidt for helpful discussions. We would also like to acknowledge the support of the UK Engineering and Physical Sciences Research Council (EP/E011136/1, EP/G007276/1), European Community's Seventh Framework Programme (FP7/2007-2013) under grant agreement no. 270843 (iQIT), the European Commission's Sixth Framework Marie Curie International Reintegration Programme (MIRG-CT-2007-046432), the Nuffield Foundation and the University of Sussex.

- 
- [1] M. D. Paine, S. Gabriel, C. G. J. Schabmueller, and A. G. R. Evans, *Sensors and Actuators A: Physical* **114**, 112 (2004), ISSN 0924-4247.
  - [2] R. Krpoun and H. R. Shea, *J. Micromech. Microeng.* **19**, 045019 (2009).
  - [3] R. Krpoun, M. Rdber, and H. Shea, in *Micro Electro Mechanical Systems, 2008. MEMS 2008. IEEE 21st International Conference on* (2008), p. 964, ISSN 1084-6999.
  - [4] B. Gassend, L. Velasquez-Garcia, A. Akinwande, and M. Martinez-Sanchez, *J. Microelectromech. S.* **18**, 679 (2009), ISSN 1057-7157.
  - [5] J.-C. Mateo-Velez, V. Inguibert, J.-F. Roussel, D. Sarraill, L. Levy, F. Boulay, E. Laffont, and D. Payan, *IEEE T. Plasma. Sci.* p. 2395 (2008), ISSN 0093-3813.
  - [6] J.-M. Siguier, V. Inguibert, P. Sarraillh, D. Sarraill, G. Murat, J. Mateo-Velez, D. Payan, and N. Balcon, *IEEE T. Plasma. Sci.* **40**, 311 (2012), ISSN 0093-3813.
  - [7] V. Inguibert, D. Sarraill, J.-C. Mateo-Velez, R. Reulet, L. Levy, F. Boulay, and D. Payan, *IEEE T. Plasma. Sci.* **36**, 2404 (2008), ISSN 0093-3813.
  - [8] D. J. Wineland, C. Monroe, W. M. Itano, D. Leibfried, B. E. King, and D. M. Meekhof, *J. Res. Nat. Inst. Stand. Tech.* **103**, 259 (1998).
  - [9] M. Keller, B. Lange, H. Kazuhiro, W. Lange, and H. Walther, *Nature* **431**, 1075 (2004).
  - [10] M. Albert, A. Dantan, and M. Drewsen, *Nat. Photonics* **5**, 633 (2011).
  - [11] L. Lorini, N. Ashby, A. Bruschi, S. Diddams, R. Drullinger, E. Eason, T. Fortier, P. Hastings,

- T. Heavner, D. Hume, et al., Eur. Phys. J. Special Topics **163**, 19 (2008).
- [12] C. Schneider, D. Porras, and T. Schaetz, Rep. Prog. Phys. **75**, 024401 (2012).
- [13] R. Islam, E. E. Edwards, K. Kim, S. Korenblit, C. Noh, H. Carmichael, G. D. Lin, L.-M. Duam, C. C. J. Wang, J. K. Freericks, et al., Nat. Commun. **2** (2011).
- [14] J. I. Cirac and P. Zoller, Phys. Rev. Lett. **74**, 4091 (1995).
- [15] H. Häffner, C. Roos, and R. Blatt, Phys. Rep. **469**, 155 (2008).
- [16] M. D. Hughes, B. Lekitsch, J. A. Broersma, and W. K. Hensinger, Contemp. Phys. **52**, 505 (2011).
- [17] C. Ospelkaus, U. Warring, Y. Colombe, K. R. Brown, J. M. Amini, D. Leibfried, and D. J. Wineland, Nature **476**, 181 (2011).
- [18] T. H. Kim, P. F. Herskind, and I. L. Chuang, Appl. Phys. Lett. **98**, 214103 (pages 3) (2011).
- [19] Q. A. Turchette, Kielpinski, B. E. King, D. Leibfried, D. M. Meekhof, C. J. Myatt, M. A. Rowe, C. A. Sackett, C. S. Wood, W. M. Itano, et al., Phys. Rev. A **61**, 063418 (2000).
- [20] D. A. Hite, Y. Colombe, A. C. Wilson, K. R. Brown, U. Warring, R. Jördens, J. D. Jost, D. P. Pappas, D. Leibfried, and D. J. Wineland, arXiv:1112.5419v1 (2011).
- [21] D. T. C. Allcock, L. Guidoni, T. P. Harty, C. J. Ballance, M. G. Blain, A. M. Steane, and D. M. Lucas, New J. Phys. **13**, 123023 (2011).
- [22] J. Labaziewicz, Y. Ge, P. Antohi, D. Leibbrandt, K. R. Brown, and I. L. Chuang, Phys. Rev. Lett. **100**, 013001 (2008).
- [23] S. X. Wang, G. H. Low, N. S. Lachenmyer, Y. Ge, P. F. Herskind, and I. L. Chuang, J. Appl. Phys. **110**, 104901 (pages 7) (2011).
- [24] J. M. Amini, H. Uys, J. H. Wesenberg, S. Seidelin, J. Britton, J. J. Bollinger, D. Leibfried, C. Ospelkaus, A. P. VanDevender, and D. J. Wineland, New J. Phys. **12**, 033031 (2010).
- [25] A. Neuber, M. Butcher, L. L. Hatfield, and H. Krompholz, J. Appl. Phys. **85**, 3084 (1999).
- [26] A. S. Pillai and R. Hackam, J. Appl. Phys. **53**, 2983 (1982).
- [27] R. A. Anderson and J. P. Brainard, J. Appl. Phys. **51**, 1414 (1980).
- [28] A. A. Avdienko and M. D. Malev, Vacuum **27**, 643 (1977), ISSN 0042-207X.
- [29] A. S. Pillai and R. Hackam, J. Appl. Phys. **58**, 146 (1985).